Catal Lett (2011) 141:78–82
DOI 10.1007/s10562-010-0446-5

Direct CO Oxidation by Lattice Oxygen on Zr-Doped Ceria Surfaces

Zongxian Yang · Zhaoming Fu · Yanning Zhang · Ruqian Wu

Received: 2 March 2010 / Accepted: 31 August 2010 / Published online: 21 September 2010
© The Author(s) 2010. This article is published with open access at Springerlink.com

Abstract Systematic density-functional calculations have been performed to address an important issue for CO oxidation on redox ceria: the role of lattice oxygen. One major findings is that CO easily grasps one lattice oxygen atom to form CO_2^- and CO_2 on CeO_2 (111) and $Ce_{0.75}Zr_{0.25}O_2$ (111) with small activation energies. Zr dopants facilitate the reduction of Ce^{+4} to Ce^{+3} and hence weaken the Ce–O bonds, which benefit the direct formation and release of CO_2.

Keywords Density-functional theory (DFT) · CO oxidation · Zr-doped ceria · Vienna ab-initio simulation package (VASP)

1 Introduction

Rational design of robust nanocatalysts for CO oxidation and NO_x reduction is crucial for many important applications such as pollution control and energy production. Owing to its particular redox properties, ceria has been extensively utilized in catalytic converters [1, 2]. Significantly, its redox performance can be further enhanced by the presence of various dopants, such as Zr^{4+}, Ca^{2+} and some noble metal [3–6]. This offers a great opportunity to control the activity and selectivity of oxide catalysts with the aid of innovative nanofabrication techniques. One of the most important tasks for fundamental research is to attain a clear understanding of mechanisms: (1) how lattice oxygen atoms contribute toward chemical reactions and, (2) how dopants modify surface activity. It is widely believed that CO directly combines with lattice oxygen atom on ceria, through the Mars–van Krevelen mechanism [7]. However, the relevant reaction dynamics has not been satisfactorily unravelled. Shapovalov and Metiu [8] recently investigated the effects of noble metal dopants (Au, Ag and Cu) on the energetics of CO oxidation on CeO_2 (111). Their density functional calculations indicate that bonds between lattice oxygen and metal atoms in oxide are significantly weakened by the presence of dopants and hence the doped CeO_2 (111) surfaces become much more active in both releasing CO_2 and healing vacancies. Chen et al. [9] also found that Au adsorption on Ce-vacancies activates O atoms nearby. In particular, releasing and restocking oxygen through the redox processes on ceria involve the Ce^{4+}/Ce^{3+} transformation and therefore it is crucial to study the effect of irreducible dopants (e.g., Zr^{4+} and Ca^{2+} dopants) on the charge state of Ce.

The present paper reports results of systematic density functional studies on the formation of CO_2 through direct combination of CO and lattice oxygen on the clean and doped ceria. Interestingly, we found a bent $CO_{2,ad}$ structure as the transition state for the reaction: CO + oxide → $CO_{2,gas}$ + deficient oxide, on the clean ceria (111) surface. Zr-dopants further weaken the Ce–O bonds in the substrate and therefore facilitate direct formation of CO + O_L →

Z. Yang (✉)
College of Physics and Information Engineering,
Henan Normal University, Xinxiang, Henan, 453007,
People's Republic of China
e-mail: yzx@henannu.edu.cn

Z. Fu
Department of Physics, Fudan University, Shanghai 200433,
People's Republic of China

Y. Zhang · R. Wu (✉)
Department of Physics and Astronomy, University of California,
Irvine, CA 92697-4575, USA
e-mail: wur@uci.edu

$CO_{2,gas}$. These findings provide clear evidence of lattice oxygen contribution toward CO oxidation on ceria, imperative for understanding of catalytic properties of oxides.

2 Methodology and Computational Details

We used the Vienna ab-initio simulation package (VASP) [10] to solve the spin-polarized Kohn–Sham equations. The exchange and correlation interaction among electrons were described at the level of the generalized gradient approximation (GGA), using the Perdew–Burke–Ernzerhof (PBE) formula [11]. The Ce-*5s5p5d4f6s*, O-*2s2p*, C-*2s2p*, and Zr-*4s4p5s4d* were treated as valence electrons while the ionic cores were represented by the projector augmented wave (PAW) potentials [12, 13]. To appropriately describe the on-site Coulomb repulsion among Ce 4f electrons, we introduced a Hubbard parameter, U, according to the GGA + U scheme [14–17]. The value of U was chosen to be 5 eV, for the best fitting against experimental results of the bulk CeO_2 and CeO_{2-x} [15, 16]. An energy cutoff of 400 eV was used for the plane wave expansion. The Monkhorst–Pack method [18], e.g., with (4 × 4 × 4) grids for the bulk CeO_2, was adopted for the Brillouin zone sampling. The lattice size and atomic positions were optimized with a criterion that requires force on each atom to be less than 0.02 eV/Å. The climbing image nudged elastic band method (CI-NEB) [19] was employed to investigate the transition states and minimum energy paths (MEP) for adsorption and oxidation of CO on CeO_2 (111).

The calculated lattice constant for the bulk CeO_2 is 5.48 Å, a value that agrees well with the experimental data, 5.41 Å [20]. The bulk $Ce_{0.75}Zr_{0.25}O_2$ was constructed by substituting one Ce in the 12-atom cubic cell of ceria with Zr, and its optimized lattice size is 5.42 Å, also in good accordance with previous theoretical value, 5.39 Å [21]. For the free CO and CO_2 molecules, it is known that GGA leads to somewhat overestimated bond lengths but appropriate formation energies. Here, the calculated formation energies of CO and CO_2 molecules are 258.9 and 202.5 kcal/mol, respectively, in good agreement with the experimental values of 259 and 191.2 kcal/mol. (c.f. [22] and references therein) Apparently, the computational approach and parameters are adequate for the description of both reactants and substrates.

We chose the (111) and (110) surfaces of clean and Zr-doped ceria to demonstrate the orientation dependence. They are two stable low index surfaces and have been extensively studied [23, 24]. It is known that CO takes the Ce site on the clean CeO_2 (111) surface but the adsorption energy is very small, 3.9 kcal/mol [25] from GGA calculations and 4.2 kcal/mol from the present GGA + U calculations. Therefore, CO molecules are highly mobile on this substrate under ambient condition. In contrast, CO tends to strongly bind to CeO_2 (110) at the O-bridge site [25, 26]. Studies of these two surfaces thus cover extremes of ceria toward catalyzing CO oxidation.

The CeO_2 (111) and $Ce_{0.75}Zr_{0.25}O_2$ (111) surfaces were modeled with periodic slabs consisting of 12 layers of Ce(Zr) and O atoms and a vacuum region of 13 Å thick in the between. Atoms in the bottom six layers were fixed at their bulk-like positions whereas those in the top six layers were fully relaxed. The CeO_2 (110) and $Ce_{0.75}Zr_{0.25}O_2$ (110) surfaces were modeled with slabs of 6 layers of Ce(Zr) and O atoms and a vacuum region of 13 Å thick. The two bottommost layers were fixed in the structural optimization procedure. Large unit cells in the lateral plane were used to mimic cases with small CO coverage.

3 Results and Discussion

It is known that CO weakly interacts with the clean CeO_2 (111) surface, with an adsorption energy of 3.9 kcal/mol and the preferential adsorption site is on top of Ce. However, this ground state adsorption geometry might not be directly relevant to the redox process of CO on oxides depicted as: $CO + O_L \rightarrow CO_{2,gas} + d_L$. Here, O_L and d_L represent lattice oxygen atom and lattice deficiency left on the substrate after the reaction, respectively. Obviously, one crucial step is the onset of the formation of O–C–O_L bonds. To explore this possibility, we investigated various metastable adsorption geometries for CO on CeO_2 (111). As a result, we found an important configuration shown in Fig. 1a that has a bent $CO_{2,ad}$ structure, formed with CO and a lattice O atom. Here, the two C–O bonds are 1.24 Å and 1.37 Å long and the O–C–O bond angle is 125.5°, indicating strong binding between CO–O_L. Through the Bader charge analysis [27], we found that the total number of valence electrons in the bent $CO_{2,ad}$ group is 17.2, which is one electron more than that of a free CO_2 molecule. We hence call this charged bent $CO_{2,ad}$ structure CO_2^- species below. Using the ground state adsorption configuration, the bent $CO_{2,ad}$ group and $CO_{2,gas} + d_L$ as initial-final geometries, the reaction path and adsorption energy were obtained through the CI-NEB approach. In Fig. 2, it is interesting to find out that the formation of the CO_2^- species is actually very close to the transition state. The activation energy, which directly determines the reaction rate, is about 14.6 kcal/mol. Therefore, this reaction has a high probability to occur under typical reaction conditions. Furthermore, total energy calculations indicate that the

reaction pathway $CO_{gas} \rightarrow CO_{ad} \rightarrow CO_2/CeO_2$ (111) $\rightarrow CO_{2,gas} + d_L$ is exothermic, with an energy gain of 9.5 kcal/mol. Clearly, the CO_2^- species prefers to desorb as a group from the CeO_2 (111) substrate for the completion of CO oxidation, after overcoming a very small energy barrier ($\sim$1.0 kcal/mol). One may perceive a reaction dynamics that CO pulls out one lattice O from the CeO_2 (111) surface and directly oxidize in gas phase. Shapovalov and Metiu [8] also found the bent CO_2 structure for CO on CeO_2(111) but they didn't mention the charge state. The presence of charge in CO_2^- is essential for its bent shape since it should behave like a NO_2 molecule which has an O–N–O bond-angle of (132° ± 3°) [28]. If we add an electron to a free CO_2 molecule, the O–C–O bond-angle also changes from 180° to 151°. The curves of density of states (DOS) of ideal, bent and adsorbed CO_2 molecule are shown in Fig. 3. Unlike a neutral CO_2 molecule, the bent CO_2 structure has a much smaller gap between the $5\sigma \rightarrow 2\pi^*$ states. The energy difference between the HOMO and LUMO states changes from $\sim$6.5 eV for a neutral CO_2 molecule to $\sim$2.5 eV for a bent CO_2 structure. This makes it much easier to host additional electrons in the $2\pi^*$ state, such as in CO_2^-. On CeO_2(111), the $2\pi^*$ state further splits to two peaks $\sim$1.0 eV apart, because of the effect of the substrate. On the other side, the formation of $CO–O_L \rightarrow CO_2^-$ also donates one electron back to oxide. Note that the single state charge density also displays contributions around the Ce atoms in Fig. 1a. This triggers complete $Ce^{4+} \rightarrow Ce^{3+}$ transformation for one Ce atom if the local symmetry is broken, and will reduce the barrier of the desorption of CO_2^- and neutral CO_2 for the completion of CO oxidation.

More dramatic effect is found when Zr dopant is introduced. Zr is irreducible and thus may substantially change the local chemistry. On the $Ce_{0.75}Zr_{0.25}O_2$ (111) surface, neutral CO_2 molecule can be directly (non-activated) formed when CO is adsorbed on top the surface O atoms that are adjacent to the Zr dopant. As shown in Figs. 1b and 4a, a straight O–C–O geometry is the most stable adsorption configuration for CO on the $Ce_{0.75}Zr_{0.25}O_2$ (111) surface, with an adsorption energy of 18.5 kcal/mol. The C–O bond length and the O–C–O angle are 1.20 Å and 179.7°, already very close to those of a free CO_2 molecule, 1.20 Å, and 180°, respectively. The Bader analysis [27] shows that the CO_2 species has 16.01 valence electrons, and thus is neutral. The first reaction step for CO oxidation on $Ce_{0.75}Zr_{0.25}O_2$ (111) can be depicted as: $CO_{ad} + O_L \rightarrow CO_{2,ad} \rightarrow CO_{2,gas} + d_L$. The energetics for the three reaction steps are given in Fig. 4a, where it is obvious that CO oxidation may take place easily since $CO_{ad} + O_L \rightarrow CO_{2,ad}$ has zero energy barrier and $CO_{2,ad} \rightarrow CO_{2,gas} + d_L$ only requires a small desorption energy, 6.5 kcal/mol.

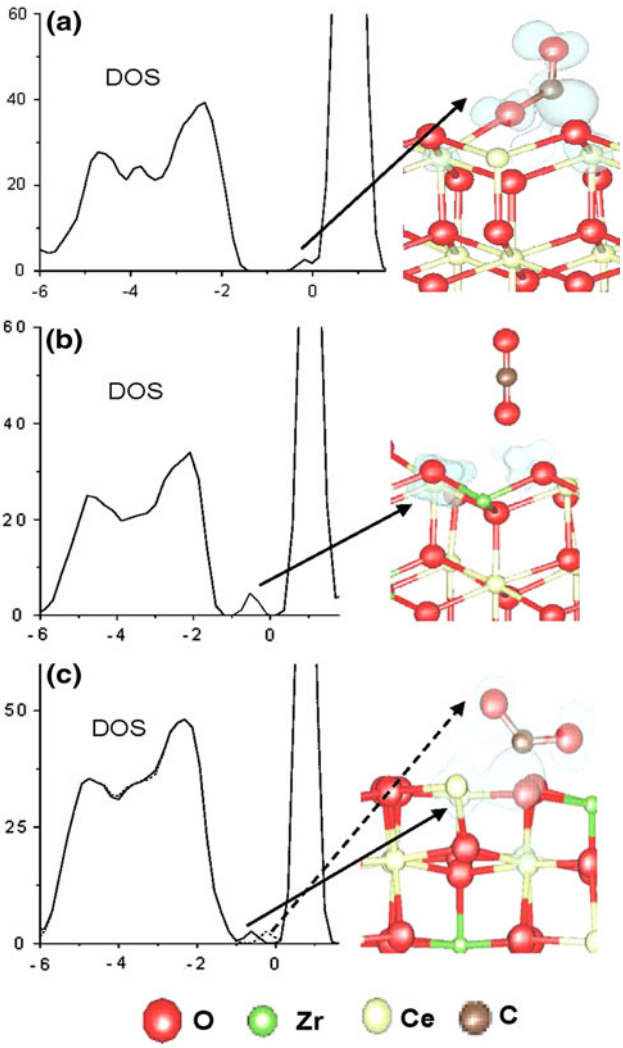

Fig. 1 Optimized structures with the density of states near the Fermi level and the distribution of the excess electrons for CO adsorbed on **a** CeO_2 (111), **b** $Ce_{0.75}Zr_{0.25}O_2$ (111), and **c** $Ce_{0.75}Zr_{0.25}O_2$ (110). All the calculations were done with spin polarization. In Fig. 1a and b, only the majority spin states are shown since the systems converged to nonmagnetic states. In *panel* **c**, the *solid and dashed curves* represent results in the majority and minority spin channels, respectively. Here and in the following figures, *yellow*, *red*, *green* and *brown* spheres represent the Ce, O, Zr, and C atoms, respectively

Apparently, Zr dopants strongly change the reaction mechanism of CO oxidation on the ceria (111) surface. Unlike the clean CeO_2 (111) surface, $Ce_{0.75}Zr_{0.25}O_2$ (111) efficiently attract CO molecules from the gas phase, as suggested by the sizable adsorption energy of 18.5 kcal/mol. On the other hand, Zr dopants reduce the energy cost for the formation of oxygen vacancy [4, 29] and thus increase the mobility of lattice oxygen atoms nearby [30]. If we define the formation energy of an O vacancy as: $E_{vac} = E(cell_{vac}) + 1/2E(O_2) - E(cell)$, where the E ($cell_{vac}$) and E (cell) are total energies of the optimized surfaces with and without an oxygen vacancy, and E (O_2) is

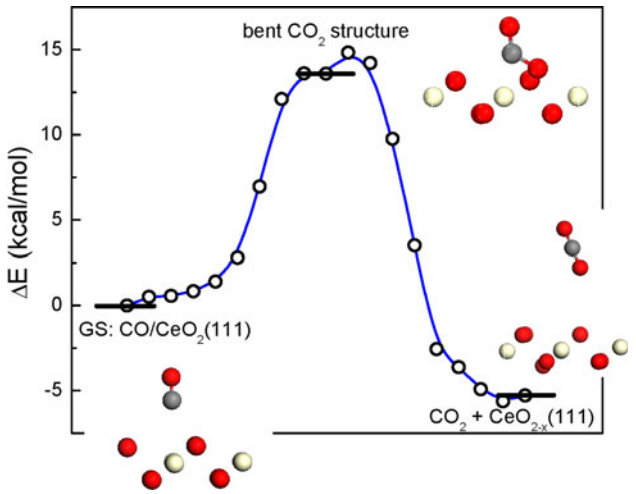

Fig. 2 The calculated energy change along the optimized reaction path for CO oxidation on CeO_2 (111) obtained through the NEB approach. *Insets* also show the atomic structures of CO adsorption state, transition state and the final state. *Red balls* are for oxygen, *grey balls* are for carbon and *white balls* are for Ce, respectively

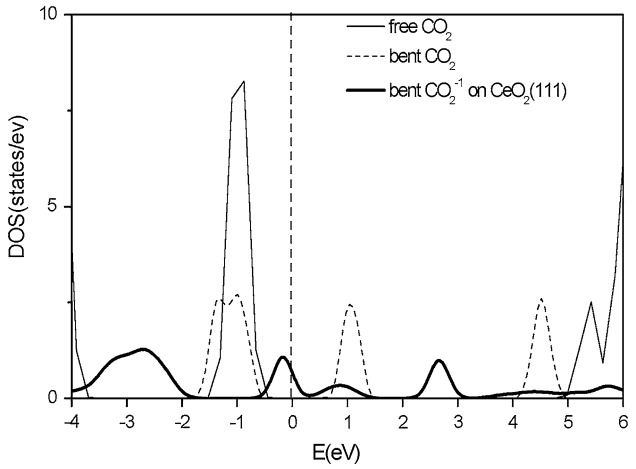

Fig. 3 The density of states (DOS) for a CO_2 molecule in gas phase (*thin solid line*), a bent CO_2 molecule (*thin dashed line*), and a bent $CO_{2,ad}^{-1}$species on the CeO_2 (111) surface (*thick solid line*)

the total energy of an oxygen molecule in the gas phase, the calculated value of E_{vac} for the undoped CeO_2 (111) surface is 2.87 eV per vacancy. By contrast, E_{vac} of the $Ce_{0.75}Zr_{0.25}O_2$ (111) surface is reduced by approximately 20% to 2.35 eV. From the DOS curve plotted in Fig. 1b, the gap state localizes on two of the Ce cations around the vacancy, indicating that the two surface Ce^{4+} cations are already reduced to Ce^{3+} cations. The surface structure is therefore somewhat distorted. In Fig. 1b, the surface Ce–O distances near the adsorption site elongated by 0.06 Å as compared to those before Zr-doping. Since the size of Ce^{3+} is larger than that of Ce^{4+}, the $CO_{2,ad}$ group is somewhat "pushed" outward for the accommodation of Ce^{3+}. Meanwhile, Zr^{4+} is smaller than Ce^{4+}, and hence provides

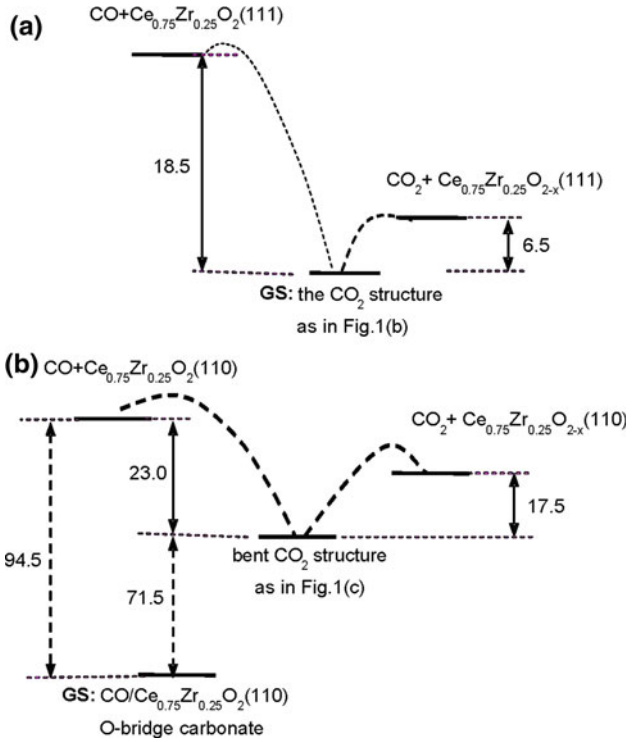

Fig. 4 Sketches of energy diagrams for CO adsorption and oxidation on **a** $Ce_{0.75}Zr_{0.25}O_2$ (111) and **b** $Ce_{0.75}Zr_{0.25}O_2$ (110). "**GS**" denotes the ground state for each system. "CO + $Ce_{0.75}Zr_{0.25}O_2$ (111)" and "CO + $Ce_{0.75}Zr_{0.25}O_2$ (110)" refer to the states of free CO molecules with clean unreduced substrates before adsorption, while "CO_2 + $Ce_{0.75}Zr_{0.25}O_{2-x}$ (111)" and "$CO_{2,gas}$ + $Ce_{0.75}Zr_{0.25}O_{2-x}$ (110)" represent the states of free CO_2 molecules with reduced substrates after CO_2 desorption

more space and releases the stress for the creation of Ce^{3+} cations. Note: The radius of Zr^{4+} (0.84 Å) is smaller than those of Ce^{4+} (0.97 Å) and Ce^{3+} (1.19 Å).

It was believed that CeO_2(110) surface is possibly more active than the CeO_2 (111) surface. In recent calculations [15, 31], it was found that O-vacancy may form more easily on the (110) surface than (111) surface of ceria and the departure of a neutral O atom leads to $Ce^{4+} \rightarrow Ce^{3+}$ transformation of two Ce atoms on CeO_2 (110) [15]. However, no metastable CO_2 configuration was found for CO on CeO_2 (110) and CO takes strong adsorption at the O-bridge site as reported before. Therefore, the conjecture that correlates the formation energy of d_L to the activity of oxides is questionable. The presence of Zr dopant promotes the $Ce^{4+} \rightarrow Ce^{3+}$ reduction and hence should assist the release of O_L, as attested by the reduction of the formation energy of oxygen vacancy. The calculated E_{vac} values are 2.30 and 0.94 eV for CeO_{2-x} (110) and $Ce_{0.75}Zr_{0.25}O_{2-x}$ (110), respectively. Indeed, a bent CO_2^- species was found on $Ce_{0.75}Zr_{0.25}O_2$ (110), as shown in Fig. 1c. It has C–O bonds of 1.26–1.28 Å long and the O–C–O bond angle of 136.1°; and it possesses 16.8 valence electrons according to

the Bader analysis. Nevertheless, as shown in Fig. 4b, the total energy of the $CO_2^-/Ce_{0.75}Zr_{0.25}O_2$ (110) configuration is 71.5 kcal/mol higher than that of the ground state (i.e. the O-bridging carbonate configuration) of $CO/Ce_{0.75}Zr_{0.25}O_2$ (110). Moreover, the reaction $CO_{ad} + O_L \rightarrow CO_{2,gas} + d_L$ on the $Ce_{0.75}Zr_{0.25}O_2$ (110) surface is endothermic and the energy cost is 17.5 kcal/mol if d_L is created at the Ce–Zr bridge site. Therefore, we believe that $Ce_{0.75}Zr_{0.25}O_2$ (110) is still inactive for direct CO oxidation, although it is somewhat better than CeO_2(110). We found that $CO_2^-/Ce_{0.75}Zr_{0.25}O_2$ (110) is spin polarized, with a net magnetic moment of 1.98 μ_B/cell. There are two pronounced peaks in the band gap, shown in Fig. 1c. The peak in the majority spin channel contains about one electron and its wave function localizes around the surface Ce cation. The peak in the minority spin channel represents the HOMO of the bent CO_2^- species, the $2\pi^*$ orbital.

Note that no NEB calculation is needed for processes shown in Fig. 4a and b since (1) the formation of the ground state $CO_{2,ad}$ structure on $Ce_{0.75}Zr_{0.25}O_2$ (111) is direct and exothermic; and (2) the bent $CO_{2,ad}$ structure is much higher in energy as compared with the adsorption state for $CO/Ce_{0.75}Zr_{0.25}O_2$ (110) so the chance to this structure is negligible.

4 Conclusion

In conclusion, we addressed an important issue for CO oxidation on redox oxides: the role of lattice oxygen, through systematic first principles studies. Unlike traditional density functional calculations, we explored metastable geometries, in particular, those with the $CO_{2,ad}$ groups. It is intriguing that CO directly forms CO_2 with the lattice O on CeO_2 (111) and $Ce_{0.75}Zr_{0.25}O_2$ (111) and desorbs easily afterward from the deficient substrate. Zr dopant can facilitate the CO oxidation process. This can be attributed to several factors: (1) the smaller size of Zr^{4+} than Ce^{4+}, which releases stress for the creation of Ce^{3+}; (2) the smaller reduction energy [4, 29]; and (3) the higher oxygen mobility of the Zr-doped ceria as compared with the pure ceria [30]. Since the binding energies of CO are rather high on the clean and Zr-doped CeO_2 (110), the reaction can be easily poisoned and the (110) surfaces remain inactive. We believe that the simple model here captures the main step of the Mars–van Krevelen mechanism of CO oxidation. Our findings satisfactorily explain experimental observations [5] and give indispensable insights for rational manipulations of composition and structure of nanocatalysts that involve oxides.

Acknowledgment This work was supported by the National Natural Science Foundation of China (grant no. 10674042) and the Innovation Scientists and Technicians Troop Construction Projects of Henan Province, China (grant no. 104200510014). RW also acknowledges support from DOE-BES (grant no. DE-FG02-04ER15611).

Open Access This article is distributed under the terms of the Creative Commons Attribution Noncommercial License which permits any noncommercial use, distribution, and reproduction in any medium, provided the original author(s) and source are credited.

References

1. Charles TC, Charles HFP (2005) Science 309:713
2. Trovarelli A (1996) Catal Rev Sci Eng 38:439–520
3. Rodriguez JA (2005) Abstracts of papers, 229th ACS national meeting, San Diego, CA, United States, 13–17 March 2005:IEC-123
4. Yang Z, Woo TK, Hermansson K (2006) J Chem Phys 124:224704
5. Masui T, Imanaka N (2003) Mater Integr 16:29–33
6. Widmann D, Leppelt R, Behm RJ (2007) J Catal 251:437–442
7. Mars P, van Krevelen DW (1954) Chem Eng Sci 3:41
8. Shapovalov V, Metiu H (2007) J Catal 245:205–214
9. Chen Y, Hu P, Lee M-H, Wang H (2008) Surf Sci 602:1736–1741
10. Kresse G, Furthmuller J (1996) Comput Mater Sci 6:15–50
11. Perdew JP, Burke K, Ernzerhof M (1996) Phys Rev Lett 77:3865–3868
12. Kresse G, Furthmuller J (1996) Phys Rev B 54:11169
13. Bloechl PE (1994) Phys Rev B 50:17953–17979
14. Anisimov VI, Zaanen J, Andersen OK (1991) Phys Rev B 44:943–954
15. Nolan M, Parker SC, Watson GW (2005) Surf Sci 595:223–232
16. Andersson DA, Simak SI, Johansson B, Abrikosov IA, Skorodumova NV (2007) Phys Rev B 75:035109
17. Pacchioni G (2008) J Chem Phys 128:182505–182510
18. Monkhorst HJ, Pack JD (1976) Phys Rev B 13:5188
19. Henkelman G, Uberuaga BP, Jónsson H (2000) J Chem Phys 113:9901
20. Eyring L (1979) In: Gschneider KA, Eyring L (eds) Handbook on the physics and chemistry of rare earths. North-Holland, Amsterdam
21. Rodriguez JA, Hanson JC, Kim J-Y, Liu G, Iglesias-Juez A, Fernandez-Garcia M (2003) J Phys Chem B 107:3535–3543
22. Hammer B, Hansen LB, Norskov JK (1999) Phys Rev B 59:7413–7421
23. Siokou A, Nix RM (1999) J Phys Chem B 103:6984–6997
24. Yang Z, Luo G, Lu Z (2007) J Chem Phys 127:074704
25. Yang Z, Woo TK, Hermansson K (2004) Chem Phys Lett 396:384–392
26. Nolan M, Watson GW (2006) J Phys Chem 110:16600–16606
27. Henkelman G, Arnaldsson A, Jonsson H (2006) Comput Mater Sci 36:254
28. Chen H (2005) Advanced inorganic chemistry. Higher Education Press, Beijing
29. Yang Z, Wei Y, Fu Z, Lu Z, Hermansson K (2008) Surf Sci 602:1199–1206
30. Nolan M, Fearon JE, Watson GW (2006) Solid State Ion 177:3069–3074
31. Yang Z, Woo TK, Baudin M, Hermansson K (2004) J Chem Phys 120:7741–7749